

Narrowband Near-Infrared Imaging of Young Planetary Nebulae and Transition Objects: Probing Core and Halo Structures

William B. Latter

IPAC/California Institute of Technology and Lick Observatory, U. C. Santa Cruz/NASA
Ames Research Center¹

Joseph L. Hora

Smithsonian Astrophysical Observatory and The Institute for Astronomy, University of
Hawaii²

Received _____, accepted _____

¹Mailing address: Infrared processing and Analysis Center, California Institute of
Technology, MS 100-22, Pasadena, CA 91125

²Mailing address: Smithsonian Astrophysical Observatory, 60 Garden Street, Cambridge,
MA 02138-1596

ABSTRACT

We have imaged several young planetary nebulae and proto-planetary nebulae in the $v = 1 \rightarrow 0$ S(1) line of molecular hydrogen at $2.12 \mu\text{m}$, the hydrogen Br γ line at $2.16 \mu\text{m}$, at nearby continuum wavelengths, and broadband to probe the structure of the halo regions and to examine detailed structure in the core. A number of studies of atomic and molecular emission from planetary and proto-planetary nebulae at millimeter, near-infrared, and visible wavelengths have revealed high velocity outflows that suggest the presence of shocks with a wide range of velocities. Moderate velocity shocks are an important excitation mechanism of molecular hydrogen. Fluorescent excitation of H₂ is also important in some planetary nebulae such as in NGC 7027 and M 2--9. The spatial distribution of the H₂ $v = 1 \rightarrow 0$ S(1) line can help to identify the important excitation mechanism in the planetary nebula.

The new images presented here have high spatial resolution and are very sensitive to low levels of emission. We compare our new data to existing imaging and spectroscopic data to give clues as to the structure and formation of planetary nebulae, the role of shocks, and the evolution of photon-dominated regions. Striking new complexity in structure, such as filaments, knots, and diffuse emission, is found in the several objects. This complexity is often difficult to understand. It is apparent that conditions required for excitation of near-infrared H₂ emission are common in planetary nebulae. We briefly consider implications of our new images to an understanding of the presence of molecular material and the evolution of these objects.

Subject headings; planetary nebulae: general ISM: molecules - ISM: structure
infrared: ISM: continuum - infrared: ISM: lines and bands - molecular

processes

i.

γ

1. Introduction

Interest in planetary nebulae has grown considerably in the past few years, in part as a result of the recognition of the importance of mass loss to the late stages of stellar evolution and to the injection of processed material into the interstellar medium. A number of studies of molecular emission from proto-planetary nebulae (PPN) at millimeter and near-infrared wavelengths now exist. The detection of molecular hydrogen from a considerable number of PNe (Zuckerman & Gatley 1988; Kastner et al. 1996; Hora, Latter, & Deutsch 1998) shows that the molecular signature of asymptotic giant branch (AGB) mass loss and the PPN phase can be found well into the evolution of PNe. H_2 emission has generally been attributed to the presence of shocks in the nebular shell, but UV pumped near-infrared fluorescence can also be important. The $\text{H}_2 v = 1 \rightarrow 0 S(1)$ diagnostic line is important for tracing structures in the nebula and its halo, giving information on jets and regions where interacting winds are shaping the nebulae. CCD observations of PNe have shown evidence at visible wavelengths of multiple shells in some objects, suggesting several phases of mass ejection from the central star (Jewitt et al. 1986). Multiple mass loss episodes are something that might be investigated in more detail through molecular observations. Most studies of molecular hydrogen emission from PNe have been carried out with low spatial resolution ($5'' - 20''$). High spatial resolution is required to reveal the nature of the emission components. For example, Graham et al. (1993a) have imaged the PN NGC 7027 at high spatial resolution in H_2 as well as $\text{Br}\gamma$, $\text{Br}\alpha$, and the $3.28 \mu\text{m}$ dust feature. Their images show H_2 to be in a thin-shell structure at a greater radius than the HII region, and at the inner edge of the CO shell. They conclude that the H_2 emission is excited by ultraviolet radiation in a photodissociation region.

It has been shown that there is a strong correlation between nebular morphology and molecular content, such that molecular (**CO** and H_2 in particular) are found, for the most

part, only in bipolar-type nebulae (e.g., Zuckerman & Gatley 1988; Huggins et al. 1996). Kastner et al. (1994, 1996; see also Latter et al. 1995) has imaged several PNe in H_2 and has suggested that some ring-like PNe are actually bipolar nebulae seen pole-on. The Galactic distribution of bipolar nebulae suggests that they have descended from relatively massive progenitor stars (Corradi & Schwarz 1995).

In this paper we present new broad and narrowband near-infrared images of young planetary nebulae acquired with a small pixel/large format camera. These data are typically of very high sensitivity. We are able to determine the morphology and total spatial extent of the emitting molecular hydrogen regions and determine the relationship of this emission to that of hydrogen Brackett γ . First, we discuss the observations and present the data.

2. Observations and Reduction

observations were made on Mauna Kea were made during two observing sessions (1995 January 21 - 22 and August 3 - 5 UT) using the University of Hawaii (UH) 2.2111 telescope and the QUick InfraRed Camera (QUIRC). QUIRC utilizes a 1024 x 1024 pixel HgCdTe “Hawaii” array (Hodapp et al. 1996). We used the telescope in the f1.0 configuration, giving a pixel size of $0''.18 \text{ pixel}^{-1}$. Measurements were made in the K' bandpass and fixed wavelength narrowband filters were used for observations of $\text{Br}\gamma$, $\text{H}_2 v = 1 \rightarrow 0 S(1)$ (1 % spectral width), and $\lambda = 2.23 - 2.29 \mu\text{m}$ continuum (2.7% spectral width). Because of the much broader bandpass of the UH continuum filter relative to the line filters, and possible H_2 line contamination, continuum subtraction requires some scaling of the data, and caution should be used when interpreting these data. Combining of the line and continuum data using a different color for each proved to add too much uncertainty, while a subtraction clearly reveals the location of bright continuum that does not match well between the two filters. We address these uncertainties when present in the sections that follow. Seeing on

Mauna Kea at $\lambda = 2.2 \mu\text{m}$ was typically $0''.5 - 0''.7$ while these data were being taken.

The final images were constructed from many short exposures that were individually sky-subtracted and flat-fielded before being shifted and averaged. For extended sources, the telescope was nodded to nearby regions of blank sky to obtain sky frames. Compact sources could be observed efficiently by rastering them on the array. In this way, one object frame acted as the sky frame for the next. The individual sky images were median-filtered and then subtracted from the individual frames at the same wavelength. Flat-field and dark frames were produced by averaging images using a flat-field screen at two different illumination levels. All of the data were reduced using standard IRAF routines. Flux calibration was determined by comparison with standard stars from Elias et al. (1982). It is important to note that there can be a contribution from $\text{He I } 3^3\text{P}^{\circ} - 4^3\text{S}$ at $\lambda = 2.114 \mu\text{m}$ in the H_2 narrowband images. In virtually all cases, such a contribution can be determined from the location of the emission. For most of the objects presented here, this He I contribution is not a problem for the interpretation of the observed emission. The data are summarized in Table 1, and filter parameters are listed in Table 2. The grayscale images are presented in Figures 1 - 8 (Plates # - # ??). Unless extended emission is found, the full field of view ($\approx 3''$) is shown only for those PN for which extended emission was seen.

3. Results and Discussion

A number of evolved PNe have what might be considered "extended" emission (emission that is found to be present beyond the region traditionally called the planetary nebula - the brightest emitting part of the ionized gas) from both atomic and molecular material (for example NGC 6720; the Ring Nebula; see e.g. Latter et al. 1995 and Kastner et al. 1994). For this study, we have investigated if any of the well-studied young PNe and PPNe have detectable extended molecular hydrogen emission. Of the objects examined,

none were found to have emission beyond that which was previously known. However, in several cases to be discussed, significantly more emission and structure was found, adding to our understanding of the large scale structure of these objects.

Additionally, these new images are of sufficiently high spatial resolution to make it possible for us to locate with precision from where in the compact nebula the previously detected emission is coming, and in some cases structure is revealed in much higher detail than was previously possible. Targets were chosen to be among the most often studied objects that also have detected H_2 emission (except one, IC 2149). In this section, we discuss the results for each object and consider the implications.

3.1. **AFGL 618**

AFGL 618 has been studied extensively at infrared wavelengths (Westbrook et al. 1975; Latter et al. 1992; Kelly, Latter, & Rieke 1992; Latter et al. 1995). Previous images have not been of sufficient spatial resolution to determine the exact location of the strong molecular hydrogen emission. Latter et al. (1995) were able to produce a continuum-subtracted image that shows the general distribution of H_2 to be within the polar regions. This is consistent with other objects of its type, such as AFGL 2688. An unusual feature of AFGL 2688 is prominent emission from H_2 in what appears to be an equatorial torus (e.g., Latter et al. 1993). It is of interest to find the origin of this emission (see §3.2) and to find if it occurs in any other objects of similar morphology and evolutionary state. Our new images of AFGL 618 go considerably deeper than previous work, so we expect them to show the location of all detectable H_2 emission from the object. No equatorial emission is found.

In Figure 1 we show the continuum-subtracted H_2 emission superimposed on the unsubtracted data. Because of the much wider spectral width of the continuum filter

compared to the H_2 filter, the quality of the subtraction] is worse at, and very near the bright continuum peak. In spite of this uncertainty, it is very clear that we have resolved the H_2 emission into the two lobes. In addition some structure within the lobes is found. There is a pronounced asymmetry of the H_2 emission in the western lobe. This asymmetry is not visible in the continuum image, but only in H_2 emission. The eastern lobe appears much more symmetric, with a peak in the emission approximately centered within the visible lobe. "Spikes" of emission at the eastern most end of the H_2 emission are likely a result of brightening near the lobe surface. This morphology indicates that molecular hydrogen is excited not only by an interacting wind shock within the lobe (the bright peak), but also UV photon excited along the inner edges of the lobe. Such a result is consistent with the findings of Latter et al. (1992), who reported that the H_2 is excited predominantly by shock heating, but there is also a component of UV-pumped fluorescence emission in a photodissociation region (PDR). Such a morphology of the PDR is clearly seen in the bipolar PN M2-9 (Hora & Latter 1994). The relatively low intensity of the fluorescent emission in AFGL 618 compared to that expected from a nearby B0 star led Latter et al. (1992) to conclude that the UV flux from the central star must be attenuated by clumps or some other similar component (see also Kelly et al. 1992; Schmidt & Cohen 1981). If the limb brightened emission at the lobe edges is the location of the PDR in AFGL 618, then the morphology would again be consistent with the findings of Latter et al. (1992). We find no evidence for the proposed clumps. However, the much smaller filling factor of the apparent PDR region compared to the shocked gas that fills most of the lobes brings into question the need for shielding of the molecular gas by clumps. The observed morphology could be caused by swept-up material during wind interactions as well. Very high spatial resolution spectroscopy of the H_2 spectrum and imaging in the brightest lines is required before the origin of the H_2 emission and the structure of AFGL 618 can be understood.

3.2. AFGL 2688

AFGL 2688 (the “Egg Nebula”; Ney et al. 1975) has been studied extensively (see Latter et al. 1993 and references therein; Sahai et al. 1997a, b). In addition to prominent H_2 emission in the polar lobes, this object has an enigmatic region of molecular hydrogen that appears as a ring-, or torus in the equatorial plane. The interpretation of this region is in debate (e.g., Skinner et al. 1997). Recent observations by HST/NICMOS of AFGL 2688 in H_2 (Sahai et al. 1997b) have not settled the issue. Because of the importance this emission has to our understanding of this object, it is valuable to image it with a wide field and in as much detail and sensitivity as possible. In addition, as initially shown by Latter et al. (1993) and Crabtree & Rodgers (1993), AFGL 2688 shows a striking “X-shaped” morphology in scattered red light (see also Sahai et al. 1997a). By determining the wavelength dependence of this scattered emission, it might be possible to gain important information about the properties of the scattering grains. Our images are deep enough to examine both of these properties, in addition to giving information about any other extended near-infrared emission not previously detected.

We display the images of AFGL 2688 in Fig. 2. The K’ image in Fig. 2a shows clearly that many of the features found in the *I*-band (Latter et al. 1993) and with HST/WFPC2 (Sahai et al. 1997a) are present at the longer wavelengths as well. The new HST/NICMOS image of Sahai et al. (1997b) hints at the presence of emission arcs in the continuum of the type seen at shorter wavelengths. This $2.2\mu\text{m}$ image clearly shows the same features well beyond the dominant polar lobes. In addition, the “X-shaped” morphology is clearly visible. However, this image shows it to be asymmetric, with the north-eastern and south-western spikes to be brighter than the opposing spikes in the same lobe. To a much lower degree, this type of asymmetry is seen in the images of Sahai et al. (1997b), but the southern lobe seems to have the opposite sense to our image here. The origin of this type of asymmetry is

not explained by the classical model for AFGL 2688 (see Latter et al. 1993) or the revised model of Sahai et al. (1997a).

The narrowband H_2 image shown in Fig. 2b and the continuum image in Fig. 2c hint that the asymmetry in the “X-shaped” features is real. The H_2 image shows this more clearly in spite of comparable signal-to-noise ratios in the continuum. This *might* suggest that the asymmetry seen in the spikes is a result of scattering of the H_2 emission itself. Such off-axis scattering requires that the H_2 emission not be centered within the lobe, which is seen. This suggestion requires verification using narrowband polarimetry observations of the line and continuum emission.

Our images show no hint of the additional off-axis H_2 emitting regions reported by Skinner et al. (1997). The existence of these new regions are a key feature to the radical new model presented in their paper. Skinner et al. briefly suggested that these additional features could be caused by ghosting in the narrowband filters. Such ghost images are a frequent problem in narrowband near-IR imaging. Our experience has shown that the bright continuum peak in AFGL 2688 can (and does) often cause ghosting in narrowband images. From our new data, we must conclude that the new H_2 features are not present in the object.

3.3. **BD+30°3639 and NGC 7027**

Our new images of BD+30°3639 and NGC 7027 (Figs. 3 and 4) are of considerably higher spatial resolution than previous data, while having a wide total field-of-view. The general results are consistent with earlier work (for detailed discussions, see Graham et al. 1993a, b; Hora et al. 1993; Cox et al. 1997; Shupe et al. 1997). No extended emission beyond that already known has been detected. The continuum subtraction only has a large

uncertainty at the location of the central star for BD+30°3639, not affecting the details of the H_2 emission. In the NGC 7027 data, the subtraction uncertainty is largest at the location of the bright ring and within the interior. Previous data has shown that there is a contribution from He I within the filter bandpass that is located at the bright ring, and that there is no H_2 emission within the ring interior (Kastner et al. 1994; Latter et al. 1995). The image shown in Fig. 3 has this region removed from the contoured data. We do not believe such a procedure has added significant uncertainty to the H_2 morphology, especially when compared to earlier data.

In BD+30°3639 relatively low-level H_2 emission is detected on the western side of the nebula in addition to that clearly seen on the eastern side. There is no evidence for H_2 emission along the north/south axis (see, also, Shupe et al. 1997). Such an asymmetry in molecular emission might be consistent with the suggestion that BD+30°3639 is predominantly a bipolar morphology. The emission peaks do not line up with the east/west (major) axis of the nebula, making it difficult to identify the exact morphology of this object from the available data. However, Shupe et al. (1997) present a careful comparison of the kinematics of various atomic and molecular components in BD+30°3639. These data likely can be fit by a highly inclined butterfly-type morphology of the excited H_2 .

Our spatial resolution for both of these objects is sufficiently high to show clearly that the H_2 emission falls, for the most part, entirely outside the ionized region, consistent with what would be expected if all of the H_2 emission arises from PDR surrounding the nebular core.

3.4. IRAS 21282 +2020 and IC 2149

The near-infrared spectral survey of PNe and PPNe by Hora, Latter, & Deustch (1998) detected IRAS 21282+2020 in H_2 - confirming the detection by Shupe et al. (1994). The images shown in Fig. 5 reveal that the H_2 emission falls within the visible, continuum-dominated part of the nebula. An apparent bright peak of H_2 emission is found at the core. However, the continuum subtraction in this region is highly uncertain and this emission peak should be considered tentative. Aside from the H_2 emission, our near-IR data show the object to be highly symmetric and slightly extended. The bright central peak is the only significant structural feature found in these data. No newly detected extended emission was found. The distribution of emitting H_2 is found only to be located on the south-western side of the nebula, similar to that seen in our BD+30°3639 data (see, also, Shupe et al. 1998). Based on available near-IR data, Latter et al. (1995) classified IRAS 21282+2020 as peculiar. These new data reveal the object more clearly. We, therefore, now suggest that the object is more closely associated with bipolar nebulae.

IC 2149 was not detected in H_2 in the spectroscopic survey of Hora et al. (1998). We also find no evidence for H_2 emission in the current imaging data (Fig. 6). The continuum subtraction appears good throughout the nebula, except at the location of the central star. This object is classified as a peculiar morphological type (Balick 1987). We do not find reason to change that classification based on our new near-infrared data. The lack of obvious bipolar morphology is consistent with the lack of detected H_2 (i. e., Kastner et al. 1996). However, the overall shape is not unlike that of other strongly bipolar objects, such as AFGL 618. Higher resolution data will be required to firmly classify this object.

3.5. M 1-16

The H_2 emission from M 1-16 is shown clearly to be extended in large bipolar lobes at least $3.5''$ from the central core (see Fig. 7). No continuum is found in the extended polar regions, and no subtraction was attempted for the core region. The morphology of the H_2 emission suggests excitation by shocks on the outer edges of a powerful bipolar outflow or jet. This interpretation is supported by observations of the fast wind reported by Sahai et al. (1994) and Schwarz (1992). However, spectra of the lobe regions suggest that interactions with UV photons is important to the excitation of the near-infrared H_2 emission (Aspin et al. 1993). We find that the molecular emission falls in apparent cones surrounding the jet-like atomic emission (see Schwarz et al. 1992; Aspin et al. 1993). There is a clear asymmetry in the emission such that the northwestern region and the southeastern region are considerably brighter than the opposing sides. An arc of emission is visible in the northern lobe. Other similar structures might be present at low flux levels. It is apparent that arcs and rings are a common feature of PN and PPN, suggesting that time-variable mass loss rates are common as well.

The core of M 1-16 is surprisingly circular in appearance. Weak emission is seen to extend a short distance away from the core in the direction of the bipolar lobes. The core appears to be just resolved, but no distinctive features are present that might help determine the origin of the polar jets.

3.6. J 900

The small scale structure in the core of J 900 is clearly highly bipolar (Fig. 8), with two well resolved lobes and a visible central star between (see, also, the detailed study of J 900 by Shupe et al. 1995). The overall core structure is very circular and symmetric in

appearance, which is in stark contrast to the large scale structure viewed in H_2 emission. An “indentation” in the l-ortll-western lobe at the location where the H_2 jet originates, suggesting a lower density wind channel in the core. There is no contribution from continuum emission to the extended H_2 emission, and no subtraction was attempted in the core.

The overall appearance of the H_2 emission is qualitatively similar to that seen in M 1-16- clear evidence for a bipolar wind, or jet, and the lobes are asymmetric in a similar way. We also find considerable highly structured emission that does not appear to be directly related to the bipolar lobes. The most prominent structure of this type is the ridge of emission to the north-west. There is a similarity of the J 900 H_2 emission to the “beams” seen in AFGL 2688 (Latter et al. 1993; Sahai et al. 1997a). But, the origin must be different - the AFGL 2688 “beams” are seen in reflected continuum, the J 900 “beams” are only seen in H_2 emission. The emission in the north-eastern lobe has non-uniform brightness that is similar to the ring structures found in AFGL 2688 and other objects. This might indicate a periodic change in mass loss rate. If this is indeed the case, then the north-eastern ridge and other emission found around the nebula could be remnants of early mass loss episodes. An alternative hypothesis is that the H_2 emission is from a toroidal disk, not from polar lobes. Such a morphology would be highly unusual when compared to objects for which the morphology is known (see, e.g., Latter et al. 1995; Kastner et al. 1996). An understanding of the H_2 kinematics of the lobes and nearby regions is required.

4. Molecular Hydrogen Excitation in Planetary Nebulae and Proto-Planetary Nebulae

A long standing problem in the interpretation of H_2 emission from interstellar and circumstellar environments is understanding the excitation mechanism. Three fundamental

mechanisms are possible. One is excitation of a near-infrared fluorescence spectrum resulting from a rotational-vibrational cascade in the ground electronic state following electronic excitation by the absorption of a UV photon in the Lyman and Werner bands (Black & van Dishoeck 1987). The other is collisional excitation in a warm gas ($T_K \gtrsim 1600$ K). While UV excitation in a low density gas produces an easily identifiable spectrum, the level populations can be driven to produce thermal line ratios when the UV flux is large and densities begin to exceed $\approx 10^4 \text{ cm}^{-3}$ (Sternberg & Dalgarno 1989). Detailed spectral and morphological analysis are often required to determine an origin of the near-IR spectrum. The formation of H_2 on the surfaces of dust grains and in the gas phase is the third excitation mechanism. While potentially important in isolated regions of certain objects, we do not consider this to be generally important in PN and proto-PN relative to the other two processes. This is because molecular formation in PN is relatively slow compared to dissociation rates.

In PN and PPN, the situation can be complicated by both dominant excitation mechanisms being present simultaneously, and in different forms. Several ways of exciting near-IR emission from H_2 have been identified as possible: direct thermal excitation in warm gas created behind moderate velocity shockwaves, direct excitation by UV photons from the hot central star, and somewhat indirectly by collisional excitation in warm gas created by rapid grain streaming (e.g. Jura & Kroto 1990), and excitation through absorption of $\text{Ly}\alpha$ photons (by an accidental resonance with the $\text{B}^1\Sigma_u^+ - \text{X}^1\Sigma_g^+$ $v = 1 - 2$ P(5) and R(6) transitions of H_2) which can be generated in a nearby strong shock (e. g., Black & van Dishoeck 1987).

The first two mechanisms have been clearly identified in several PN, such as thermal excitation in AFGL 2688 (e. g., Hora & Latter 1994; Sahai et al. 1997a), pure UV excitation in a low density gas around Hubble 12 (e. g., Dinerstein et al. 1988; Hora & Latter 1996;

Luhman & Rieke 1996), and UV excitation in a high density gas in M 2-9 (Hora & Latter 1994) and NGC 7027 (Graham et al. 1993b; see also Hora et al. 1995). A combined spectrum was found from a detailed analysis of AFGL 618 (Latter et al. 1992). While the form of the excitation might be clear for these and other objects, it is not always evident what is the source of the warm gas or UV photons. Winds are present in AFGL 2688 that could directly shock heat the gas, but considerable grain streaming is likely taking place as well (see Jura & Kroto 1990).

Very fast winds and dissociating shocks are present in AFGL 618, M 2-9 (e.g., Kelly, Latter, & Hora 1997), and M 1-16 (Sahai et al. 1994; Schwarz 1992) and all show clear evidence of UV excitation. In addition, the photon path to the H_2 emitting regions is not clearly in a direct line-of-sight to the central star, which for photons coming from the central star suggests scattering in what is a fairly low density medium. Alternatively, we are seeing in each of these objects excitation of H_2 at the bipolar lobe walls by UV photons generated within strong shocks produced by the fast winds. This hypothesis was explored by Latter et al. (1992) in AFGL 618, but the high relative intensity of the thermally excited emission, and rather poor spatial resolution limited this analysis. The presence of very fast winds in the lobes of each of these objects, and the presence of UV excited H_2 emission at the lobe walls strongly suggests that indirect excitation of the H_2 is occurring by interactions with photons generated by wind produced shockwaves. Detailed modeling of sensitive, high spatial resolution spectra is required. It is also evident, in general, that without detailed spectra, H_2 is a rather poor diagnostic of overall conditions in PN and PPN.

If we conclude that all of the ways to excite H_2 in PN and PPN listed above are present and important, what does this imply for our understanding of these objects and the utility of H_2 as a diagnostic? It is now well understood that the presence of molecular emission from PN and PPN is tied to the morphology of the objects such that if molecular emission

is present, the object has a bipolar morphology (e. g., Zuckerman & Gatley 1988; Latter et al. 1996; Kastner et al. 1996; Huggins et al. 1997, and references therein). Does this suggest that H_2 can be more easily excited in a bipolar nebula? We have argued that H_2 emission is excited in multiple ways in PN and PPN. While special conditions are required for H_2 emission to be seen in near-IR spectra, the conditions that drive the excitation are common in all PN and PPN and are not clearly dependent on morphological type. A *conclusion* that can be drawn from this argument alone is that molecular material is present in nebulae with a bipolar morphology and significant amounts of molecular material is *not* present in other morphological types. Therefore, objects that have a bipolar morphology must have a dense, high mass envelope in which the molecular material can be shielded and survive dissociation for relatively long times - suggesting a high mass loss rate and a high mass progenitor star. A correlation between bipolar morphology and high mass progenitor stars has been found by others (e.g., Corradi & Schwarz 1994). It seems clear that the presence of H_2 emission in a PN is not tied directly to the morphology, but that the bipolar morphology is intimately related to the density and mass of the circumstellar envelope, and therefore the mass of the progenitor star. Why high mass, high mass loss rate asymptotic giant branch stars shed material in an axisymmetric, but not spherical way remains a mystery.

This discussion has been general in nature. Emphasis is placed on the morphology relationships and previously published supporting data. We will revisit this argument with quantitative analysis in the forthcoming presentation of the near-IR spectroscopic survey of PN and proto-PN (Hora et al. 1995).

5. Summary

We have presented new broad and narrow band near-infrared images of several young planetary nebulae and proto-planetary nebulae. These images have high spatial resolution

and are very sensitive to low levels of emission. A goal of this work was to search for faint extended continuum or H_2 line emission. A significant result is that no previously unidentified extended emission was found. In addition, extended emission around J 900 and M 1-16 is now clearly seen and the morphology identified. The origin of the detailed and complex structures now seen in J 900 are not easily understood. M 1-16 has two bipolar lobes that are seen in these data only in molecular hydrogen emission. When compared with other data, it is evident that these lobes are the result of shocks in wind swept gas surrounding bipolar jets.

New complexity is seen in the bipolar proto-planetary nebulae AFGL 2688 and AFGL 618. These data have cleanly resolved AFGL 618 into two well-defined lobes much like AFGL 2688, with the H_2 emission contained entirely within the lobes. Departures from bipolar symmetry are seen in both of these objects, as well as in M 1-16 and J 900. Our results for NGC 7027 and BD+30°3639 are consistent with earlier results. The enhanced spatial resolution provides a better understanding of the structure in the photodissociation region of these objects.

We have discussed (using arguments that are not entirely new) that molecular hydrogen in PN and PPN can be excited directly by UV photons from the hot central star, in shocks generated by moderate velocity winds, and by grain streaming. In addition, we make the argument that H_2 is often excited indirectly in the presence of strong shockwaves generated by a relatively large and unattenuated flux of $\text{L}\alpha$ photons coming from the shock region. This might explain the apparent UV excited emission coming from large distances from the central star, and without a direct line-of-sight view of it. This mechanism could be important for objects that include M 1-16, AFGL 618, and M 2-9. In any case, it is evident that the presence of H_2 emission in bipolar and butterfly-type nebulae must be because of a high molecular mass in the circumstellar envelope, not because of special excitation in

these types of nebulae.

The complex and often strange shapes found (especially those seen in molecular hydrogen emission) for young planetary nebulae and proto-planetary nebulae add to the menagerie of shapes seen for older planetary nebulae. The evolutionary paths of these shapes are not clear. In many cases, we are likely seeing complex H_2 structure that are relatively short lived. Such emission can occur as new winds start to blow, and dissociating ultraviolet photons begin to penetrate the extended circumstellar material through wind opened holes in an expanding envelope. The study of processes that occur at the onset of the planetary nebula phase must be done at all available wavelengths and with the highest possible resolution. When combined with existing and new ground and space acquired data, including visible, mid-infrared, and millimeter/submillimeter and radio interferometer data, the data presented in this paper will add important pieces to the puzzle of post-asymptotic giant branch evolution.

The authors are happy to thank John Black, David Shupe, and Doug Kelly for important discussions. We also acknowledge interesting conversations with Christopher Skinner. We will miss his comments and criticism. W.B.L. was supported during part of this study by a National Research Council Research Associateship. We also acknowledge support from NASA grant 399-20-61 from the Long Term Space Astrophysics Program.

Table 1

Summary of Observations

#	Object	PN G # ¹	Type ²	Filters	Fig.
1	BD+30°3639	064.7 +05.0	early round	H ₂ , Br γ , cont	3
2	NGC 7027	084.9 --03.4	inid.elliptical	H ₂ , Cent	4
3	I21282+5050	---	bipolar? ^{3,4}	H ₂ , cont	5
4	IC 2149	166.1 +10.4	peculiar	H ₂ , Cent	6
5	AFGL 618	166.4 -06.5	bipolar ^{3,4}	H ₂ , Br γ , Cent	1
6	AFGL 2688		bipolar ^{3,4}	K', H ₂ , cont	2
7	J 900	194.2 +02.5	bipolar ^{3,4}	H ₂ , Br γ , cent	8
8	M 1-16	226.7+ 5.6	bipolar ^{3,4}	H ₂ , Br γ , cent	<u>7</u>

¹Strasbourg-ESO Planetary Nebula catalog number (Acker et al. 1992).²From Balick (1987) for objects which appear in both data sets.³Not in Balick (1987).⁴See also Latter et al. (1993).

Table 2
QUIRC Filter Parameters

Filter	Half-Power Wavelengths (pm)
K	2.211 ± 0.20
H ₂	2.1132 – 2.1367
Br γ	2.1646 – 2.2053
continuum	2.230 – 2.290

REFERENCES

- Acker, A, Marcout, J., Ochsenbein, F., Scholu, C., Stenholm, B., & Tylenda, R. 1992, The
Strasbourg-ESO Catalogue of Galactic Planetary Nebulae (München: ESO)
- Aspin, C., et al. 1993, *A&A*, 278, 255
- Balick, B. 1987, *AJ*, 94, 671
- Black, J. H., & van Dishoeck, F. F. 1987, *ApJ*, 322, 412
- Corradi, R. I. M., & Schwarz, H. E. 1995, *A&A*, 293, 871
- Cox, P., Maillard, J.-P., Huggins, P. J., Forveille, T., Simons, D., Guiloteau, S. Riguat, F.,
Bachiller, R., & Omont, A. 1997, *A&A*, 321, 907
- Crabtree, D., & Rogers, C. 1991, *BAAS*, 23, 911
- Dinerstein, H. L., Lester, D. F., Carr, J. S., & Harvey, P. M. 1988, *ApJ*, 327, L27
- Elias, J. H., Frogel, J. A., Mathews, K., & Neugebauer, G. 1982, *AJ*, 87, 1029
- Graham, J. R., Herbst, T. hi., Matthews, K., Neugebauer, G., Soifer, '1., Serabyn, E., &
Beckwith, S. 1993b, *ApJ*, 40S, 1,105
- Graham, J. R., Serabyn, E., Herbst, T. hi., Matthews, K., Neugebauer, G., Soifer, B. '1.,
Wilson, T. D., & Beckwith, S. 1993a, *AJ*, 105, 250
- Hodapp, K.-W., et al. 1996, *New Astron.*, 1, 177
- Hora, J. L., Deutsch, L. K., Hoffman, W. F., Fazio, G. G., & Shivanandan, ii. 1993, *ApJ*,
413, 304
- Hora, J. L., & Latter, W. B. 1994, *ApJ*, 437, 281
- Hora, J. L., Latter, W. B., & Deustch, L. K. 1998, *ApJ*, in preparation]]
- Jura, h4., & Kroto, II. 1990, *ApJ*, \$51, 222

- Kastner, J. H., Gatley, I., Merrill, K. M., Probst, R., & Weintraub, D. A. 1994, ApJ, 421, 600
- Kastner, J. H., & Weintraub, D. A. 1994, ApJ, 434, 719
- Kastner, J. H., Weintraub, D. A., Gatley, I., Merrill, K. M., & Probst 1996, ApJ, 462, 777
- Kelly, D. M., Latter, W. B., & Rieke, G. H. 1992, ApJ, 395, 174
- Kelly, D. M., Latter, W. B., & Hora J. H. 1998, in preparation
- Latter, W. B., Maloney, P. R., Kelly, D. M., Black, J. H., Rieke, G. H., & Rieke, M. J. 1992, ApJ, 389, 347
- Latter, W. B., Hera, J. L., Kelly, D. M., Deutsch, L. K., & Maloney, P. R. 1993, AJ, 106, 260
- Latter, W. B., Kelly, D. M., Hora, J. L., & Deutsch, L. K. 1995, ApJS, 100, 159
- Luhman, K., & Rieke, G. H. 1996, ApJ, 461, 298
- Ney, E. P., Merrill, K. M., Becklin, E. E., Neugebauer, G., & Wynn-Williams, C. G. 1975, ApJ, 19S, L129
- Sahai, R., et al. 1997a, ApJ, in press
- Sahai, R., Hines, D., & Rieke, M. et al. 1997 b, apj, in press
- Sahai, R., Wootten, A., Schwarz, H. E., & Wild, W. 1994, ApJ, 42S, 237
- Schmidt, G. D., & Cohen, M. 1981, ApJ, 246, 444
- Schwarz, H. E. 1992, A&A, 264, L1
- Shupe, D. L., Armus, L., Knop, R. A., Larkin, J. E., Matthews, K., & Soifer, B. T. 1994, BAAS, 185, -47.04
- Shupe, D. L., Armus, L., Matthews, K., & Soifer, B. T. 1995, AJ, 109, 1173

Shupe, D. L., Larkin, J. E., Knop, R. A., Armus, L., Matthews, K., & Soifer, B. T. 1997,
ApJ, submitted

Skinner, C. J., et al. 1997, A&A, 328, 290

Sternberg, A., & Dalgarno, A. 1989, ApJ, 338, 197

Westbrook, W. E., Becklin, E. E., Merrill, K. M., Neugebauer, G., Schmidt, M., Willner, S.
P., & Wynn-Williams, C. G. 1975, ApJ, 202, 407

Zuckerman, B., & Gatley, I. 1988, ApJ, 324, 501

Fig. 1.- **a:** AFGL 618 in $2.121\ \mu\text{m}$ H_2 emission. This image is dominated by continuum within the filter bandpass. A continuum subtraction shows clearly the location and morphology of the H_2 emission (contours). There is some uncertainty in the continuum subtraction near the bright continuum peak (see text). **b:** As in **a** but for $2.16\ \mu\text{m}$ hydrogen $\text{Br}\gamma$ emission. The spatial extent of the $\text{Br}\gamma$ emission is unresolved in these data (contours). In these and all other figures, north is up and east is to the left, and the units on the grayscale wedge are $\log_{10}(\text{Jy pixel}^{-2})$ for a pixel size of $0''.18$ pixel $^{-1}$.

Fig. 2--- AFGL 2688 in several near-infrared filters: **a: K'**; **b:** Narrowband $2.121\ \mu\text{m}$ H_2 filter; **c:** adjacent continuum; **d:** Continuum subtracted data (contours) on the image in **b**.

Fig. 3----- a: BD+30°3639 in the $2.121\ \mu\text{m}$ H_2 filter. This image is dominated by continuum emission in the filter bandpass, but H_2 emission can be seen on the eastern side. **b:** As in **a**, but for the continuum filter. **c:** The continuum subtracted data (contours) on the image in **a**. Continuum subtraction is most uncertain within the bright ring (see text).

Fig. 4---- **a:** NGC 7027 in the $2.121\ \mu\text{m}$ H_2 filter. Continuum emission in the filter bandpass dominates only within the bright ring. All emission external to the ring appears to be H_2 emission. **b:** As in **a**, but for the continuum filter. **c:** The continuum subtracted data (contours) on the image in **a**. As for BD+30°3639, continuum subtraction is most uncertain within the bright ring (see text).

Fig. 5 --- A $2.121\ \mu\text{m}$ H_2 image of IRAS+21282+5050. The image is dominated by continuum in the filter bandpass (gray scale). A continuum subtraction shows the location of the brightest H_2 emission (contours). The enhanced peak of emission coincident with the bright continuum peak should be considered tentative, but the extended emission is well detected.

Fig. 6--- IC 2149 in the $2.121 \mu\text{m H}_2$ filter. No H_2 is detected in these data. IC 2149 has a complex near-infrared structure with no well defined bipolar, elliptical, or other types of “standard” morphologies.

Fig. 7.-- **a:** MI-16 in the $2.121 \mu\text{m H}_2$ filter. Continuum emission dominates only in the core region. All of the bipolar emission external to the core is H_2 emission. **b:** As in **a**, but for the continuum filter. **c:** A $2.16 \mu\text{m}$ hydrogen $\text{Br}\gamma$ image of MI-16. There is no resolved differences between the $\text{Br}\gamma$ emission and continuum.

Fig. 8.-- **a:** J 900 in the $2.121 \mu\text{m H}_2$ filter. It is similar to MI-16 (Fig. 7) in that the continuum emission dominates only in the core region. The H_2 emission in this object shows a complex bipolar structure with associated extended emission (see text). **b:** As in **a**, but for the continuum filter. **c:** The continuum image zoomed onto the core region. There appears to be a “dent” in the north-western lobe at the position where the extended H_2 emission originates. The low level emission extending in the direction of the north-western H_2 lobe is likely H_2 line emission that falls within the filter bandpass.

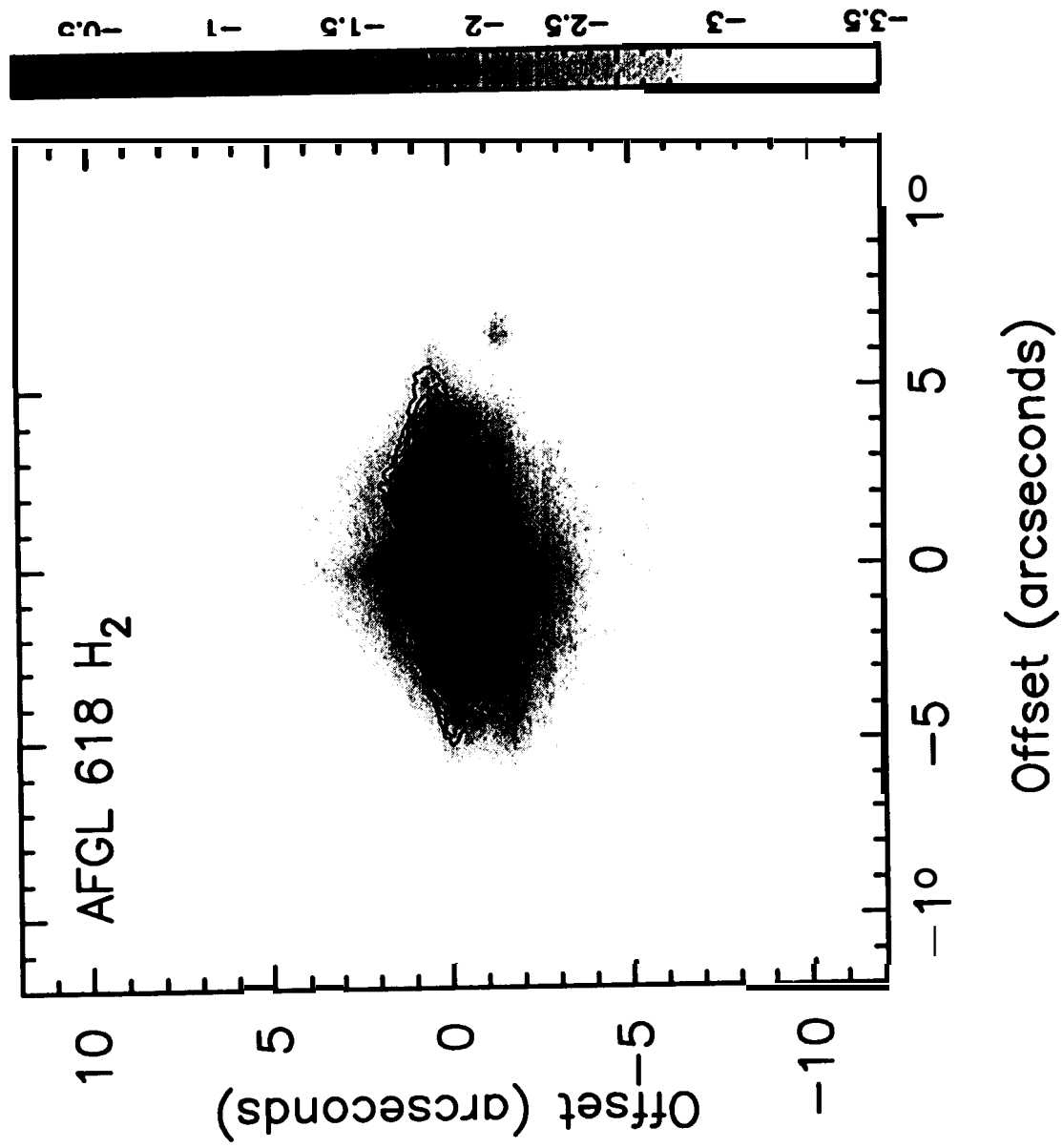
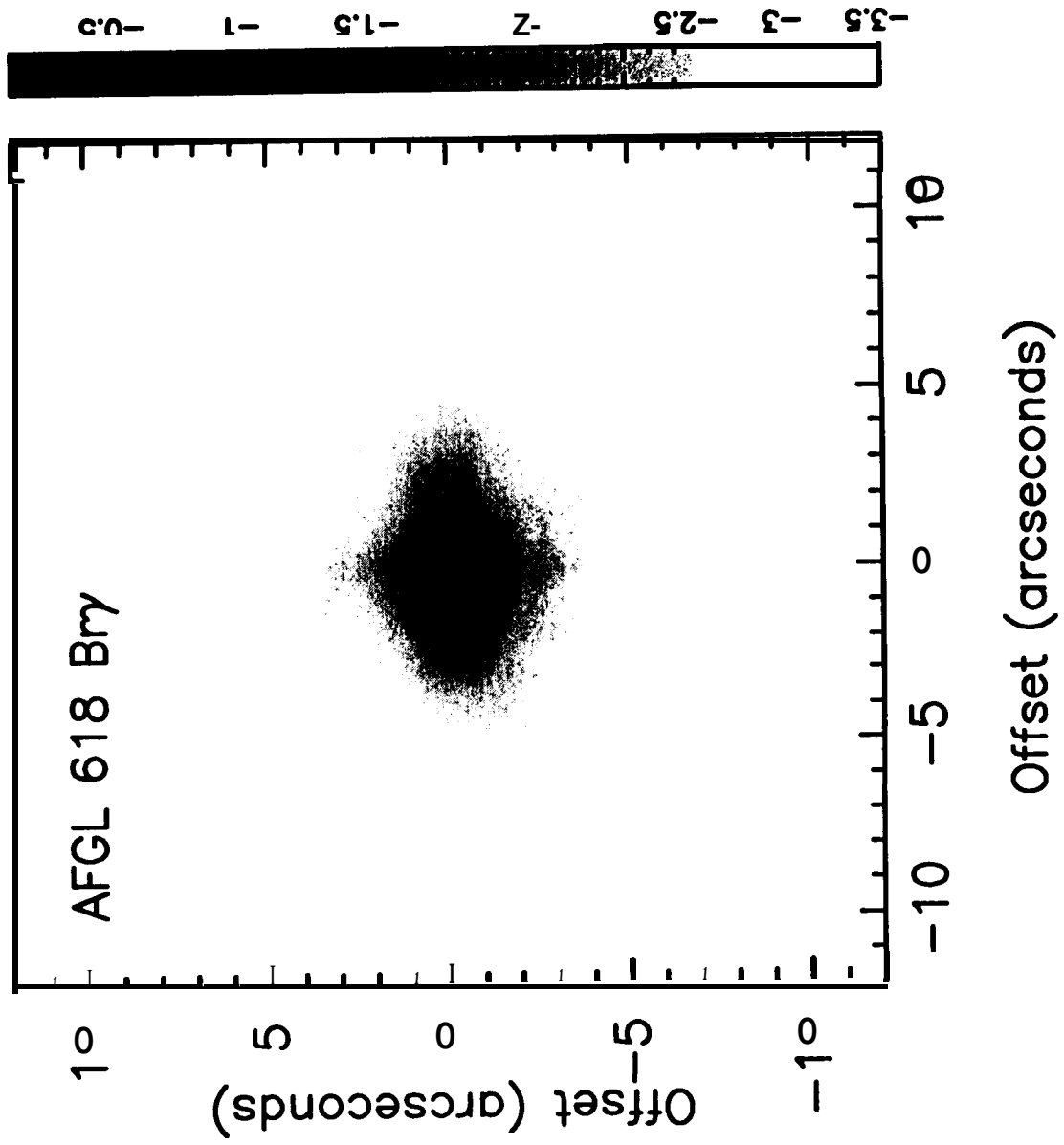
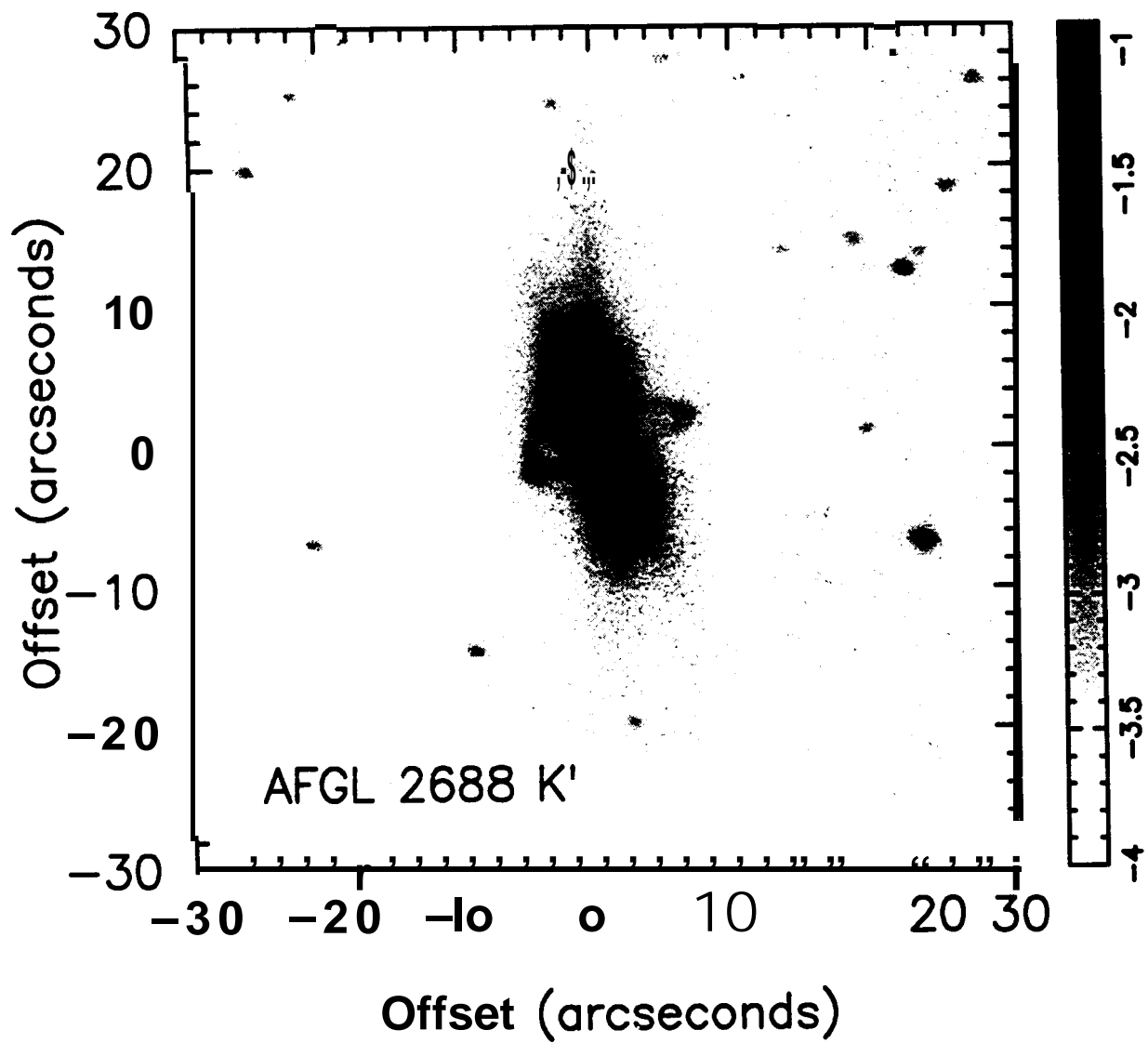
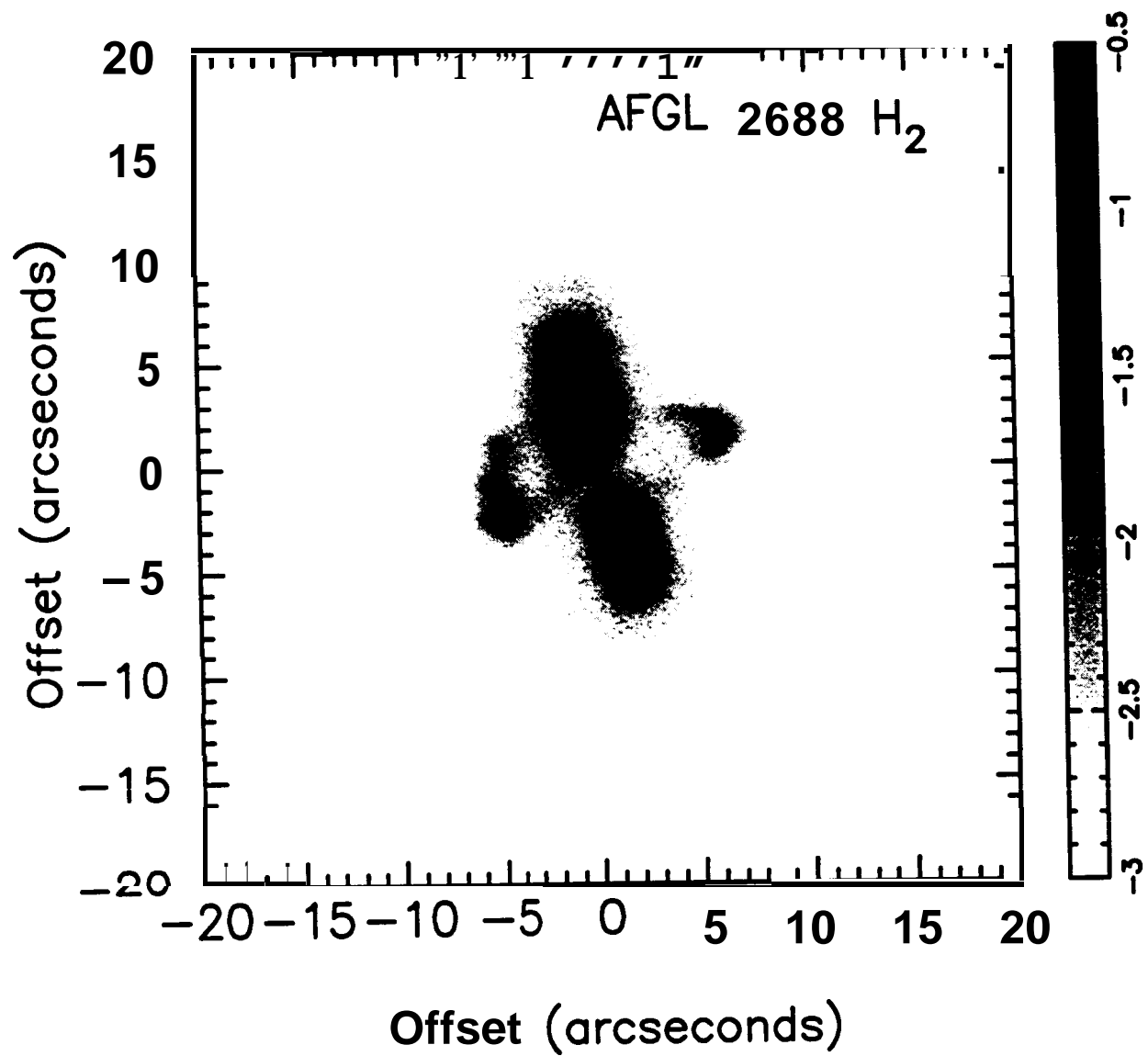
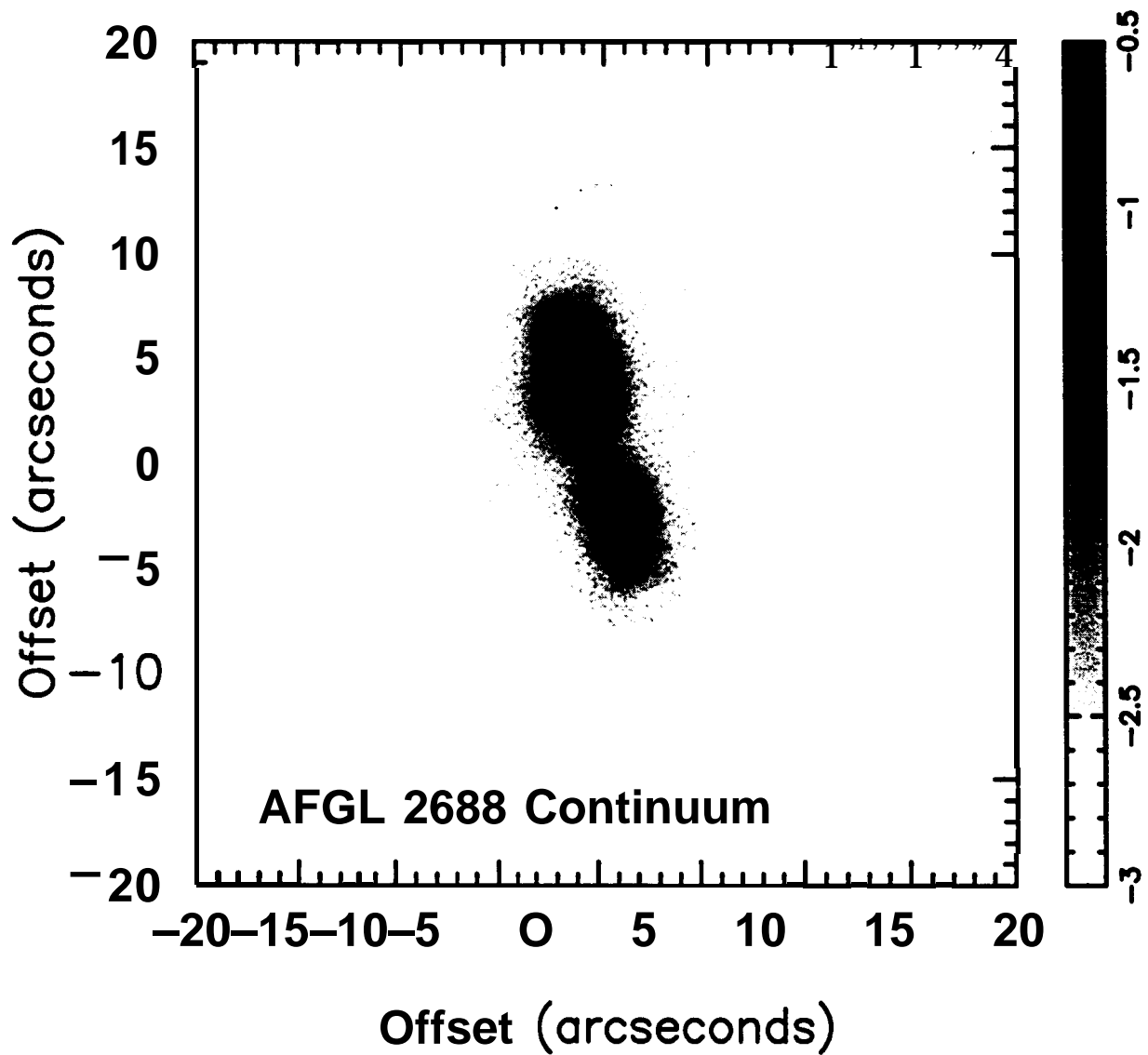


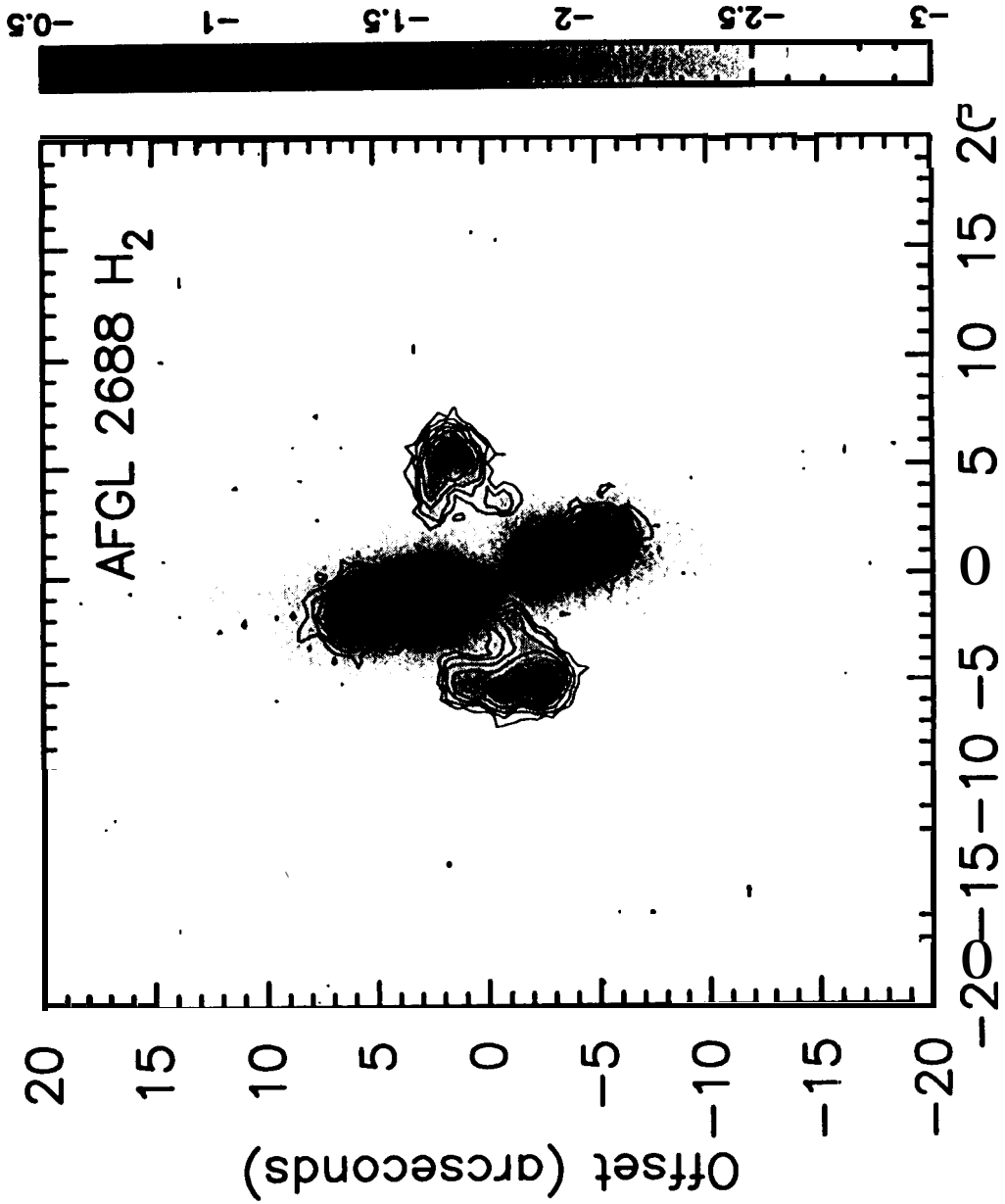
Fig. 1a

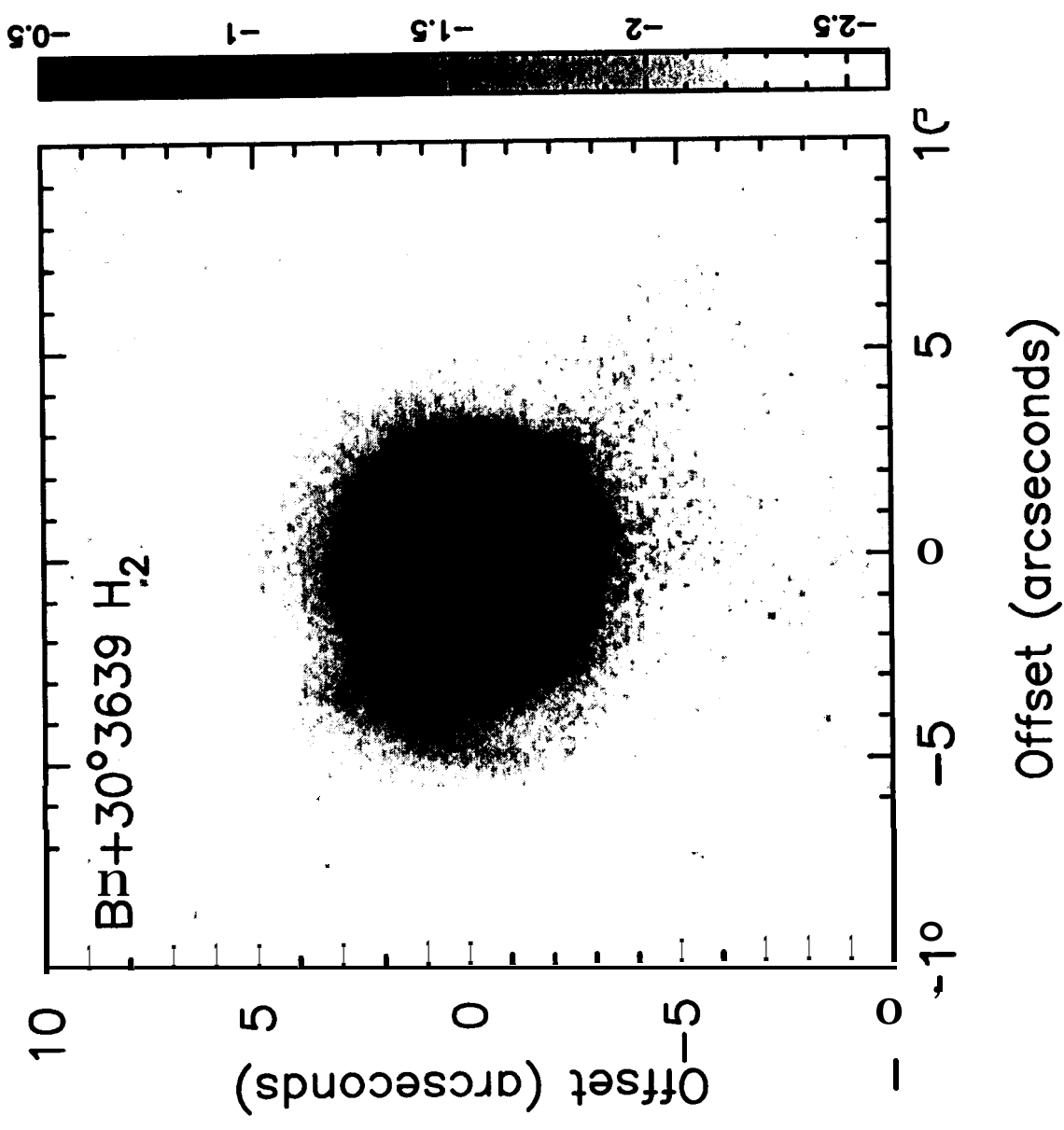


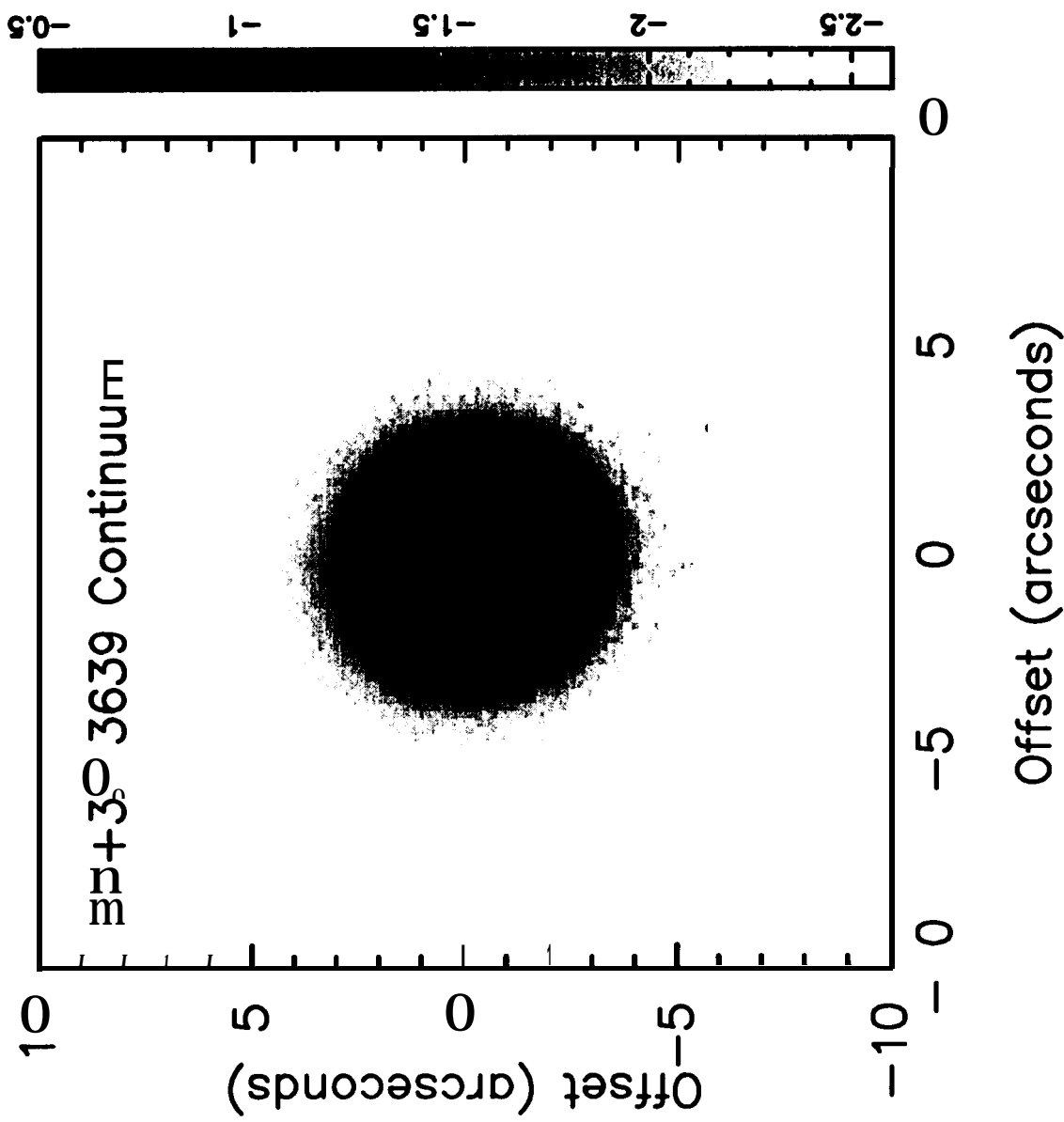


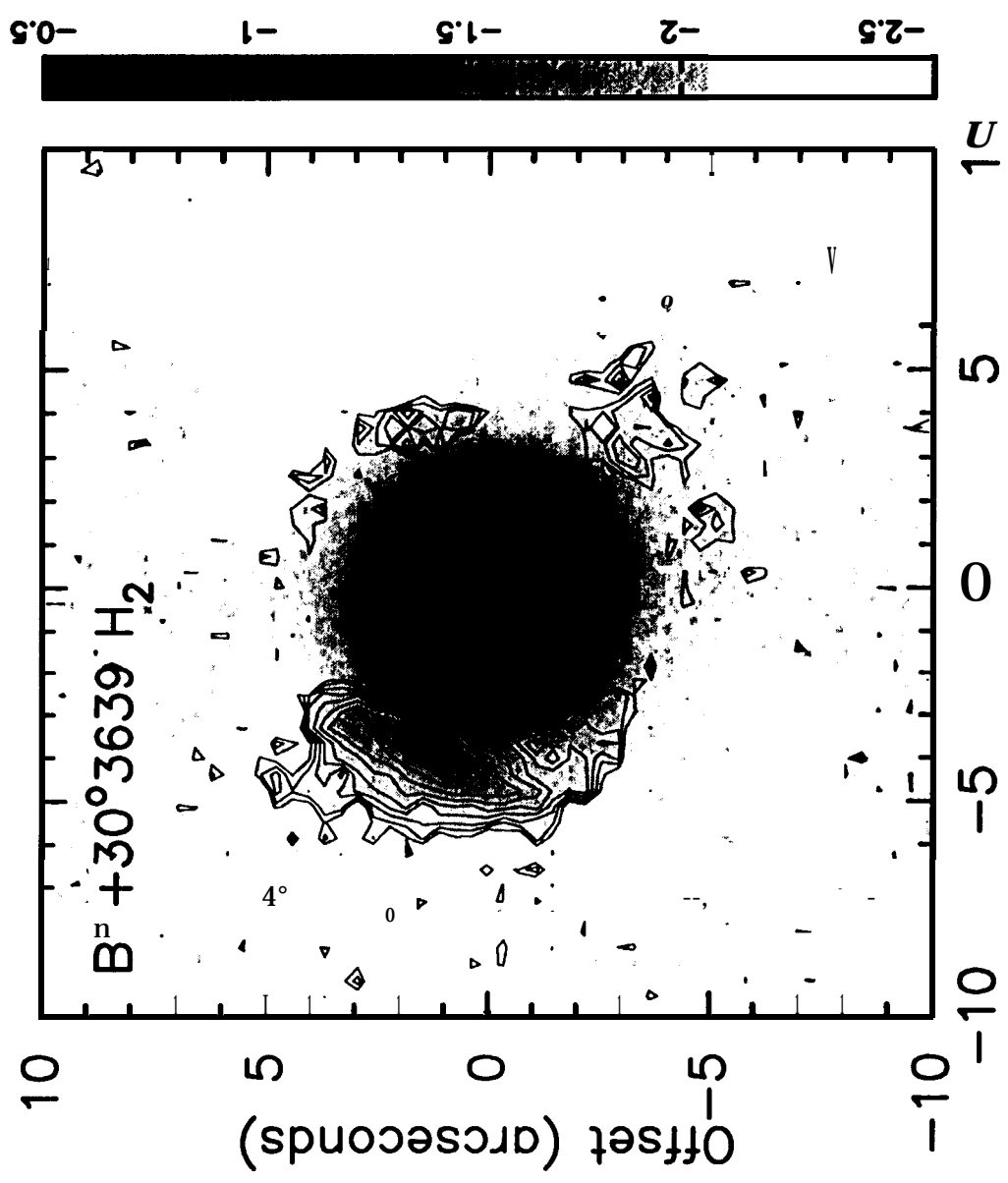




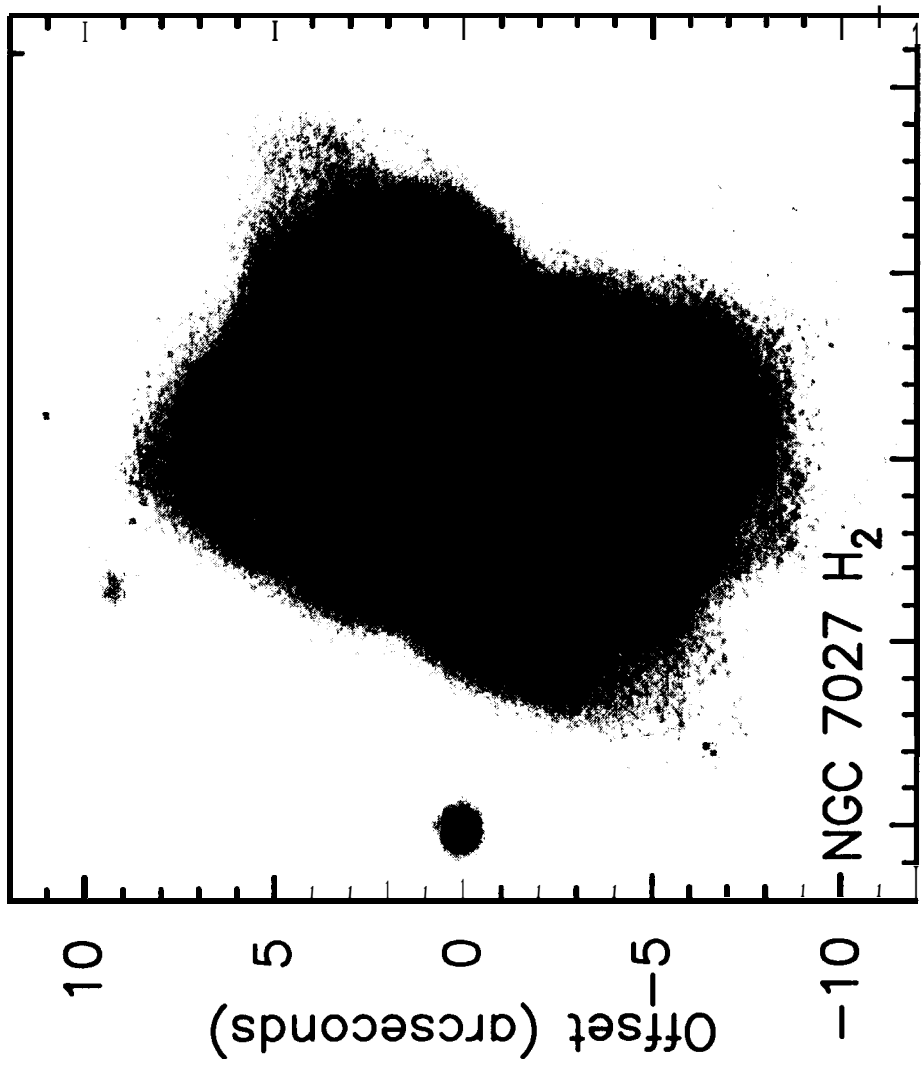
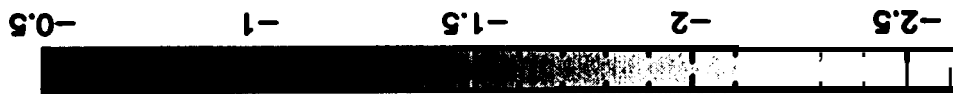




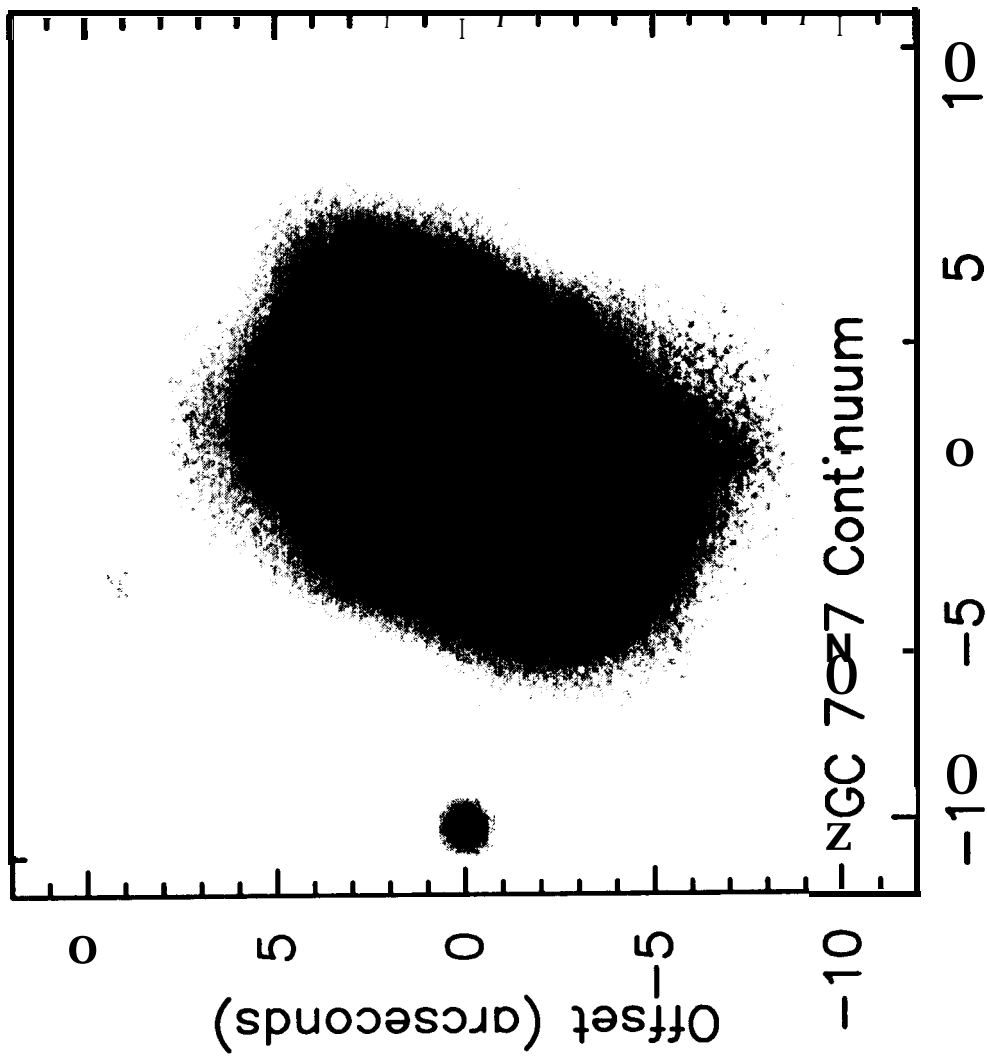
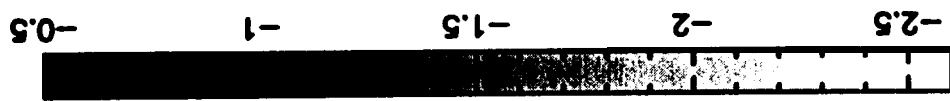




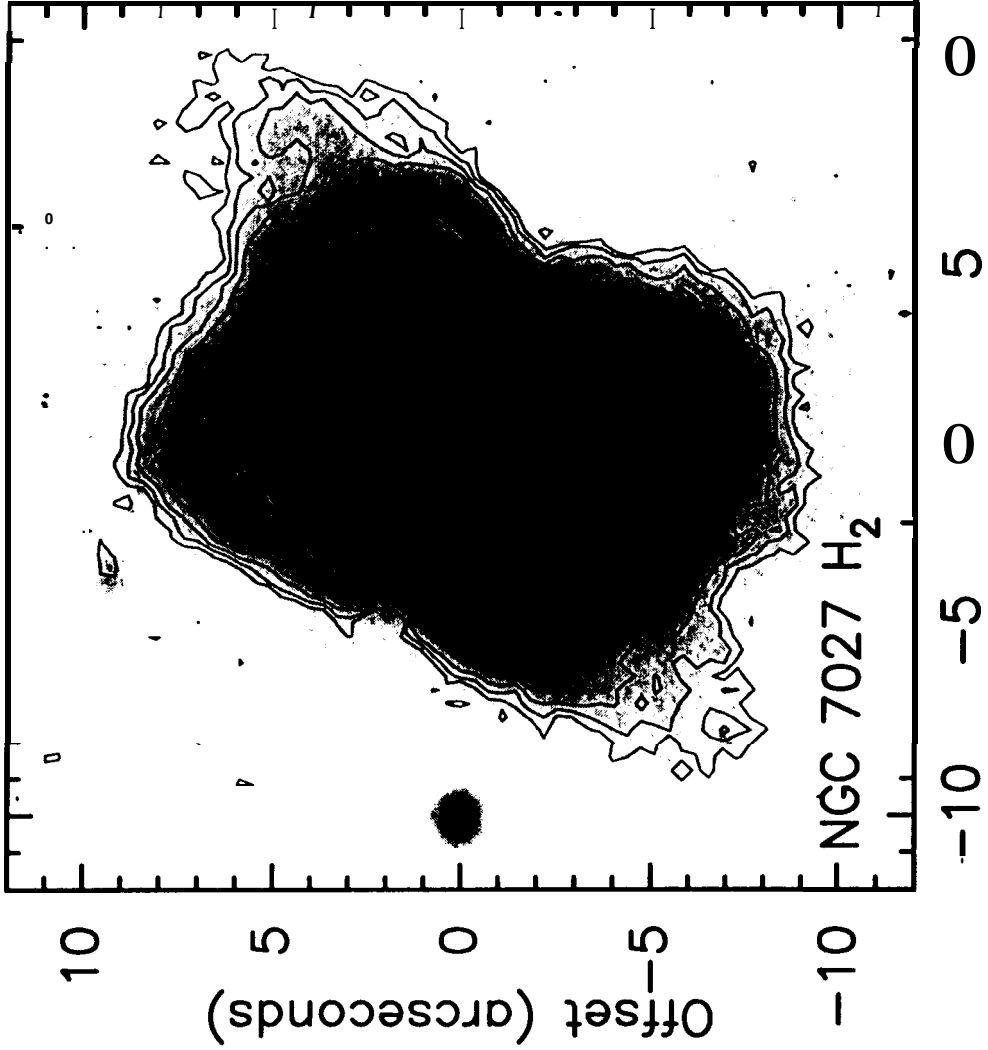
Offset (arcseconds)

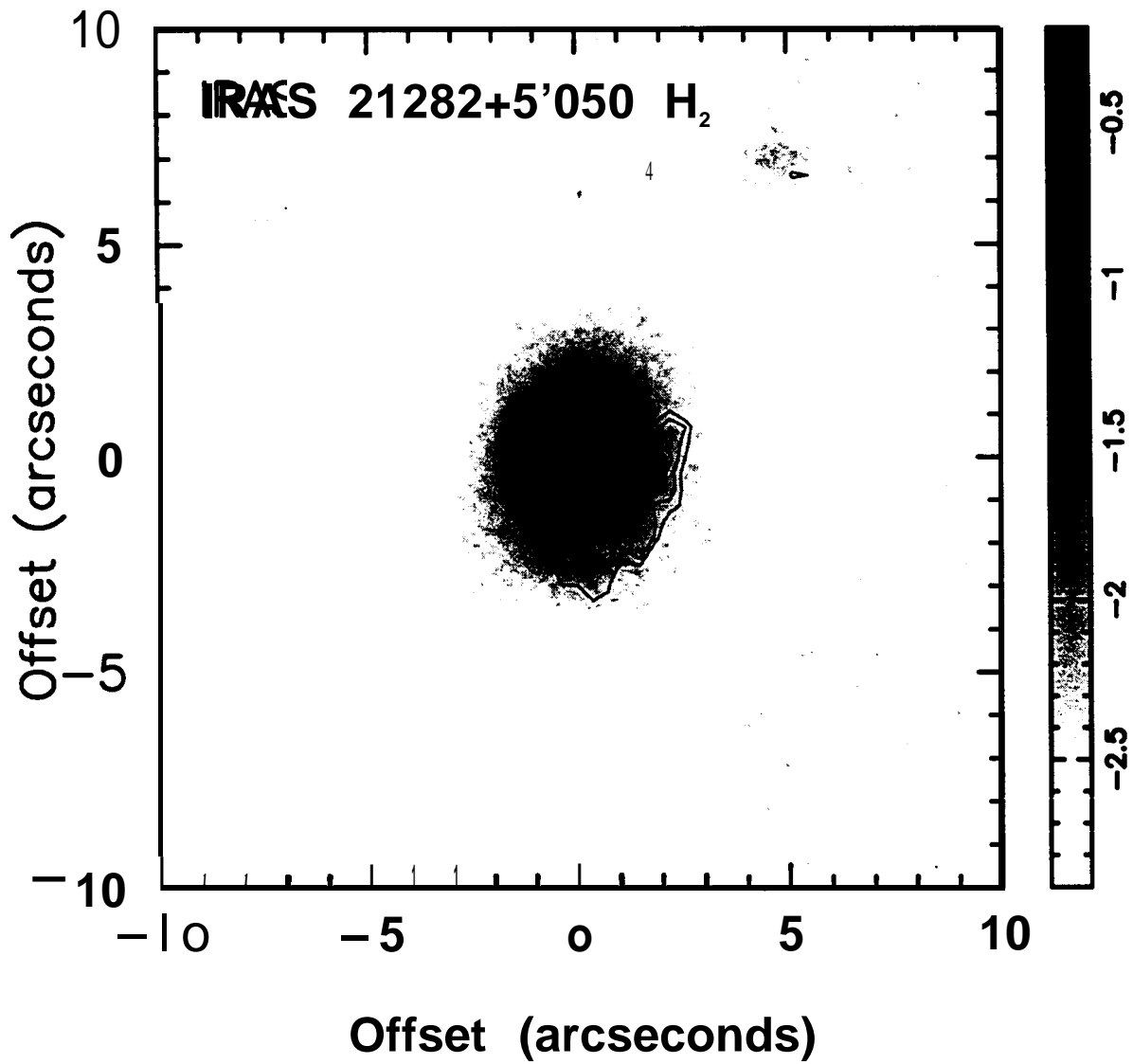


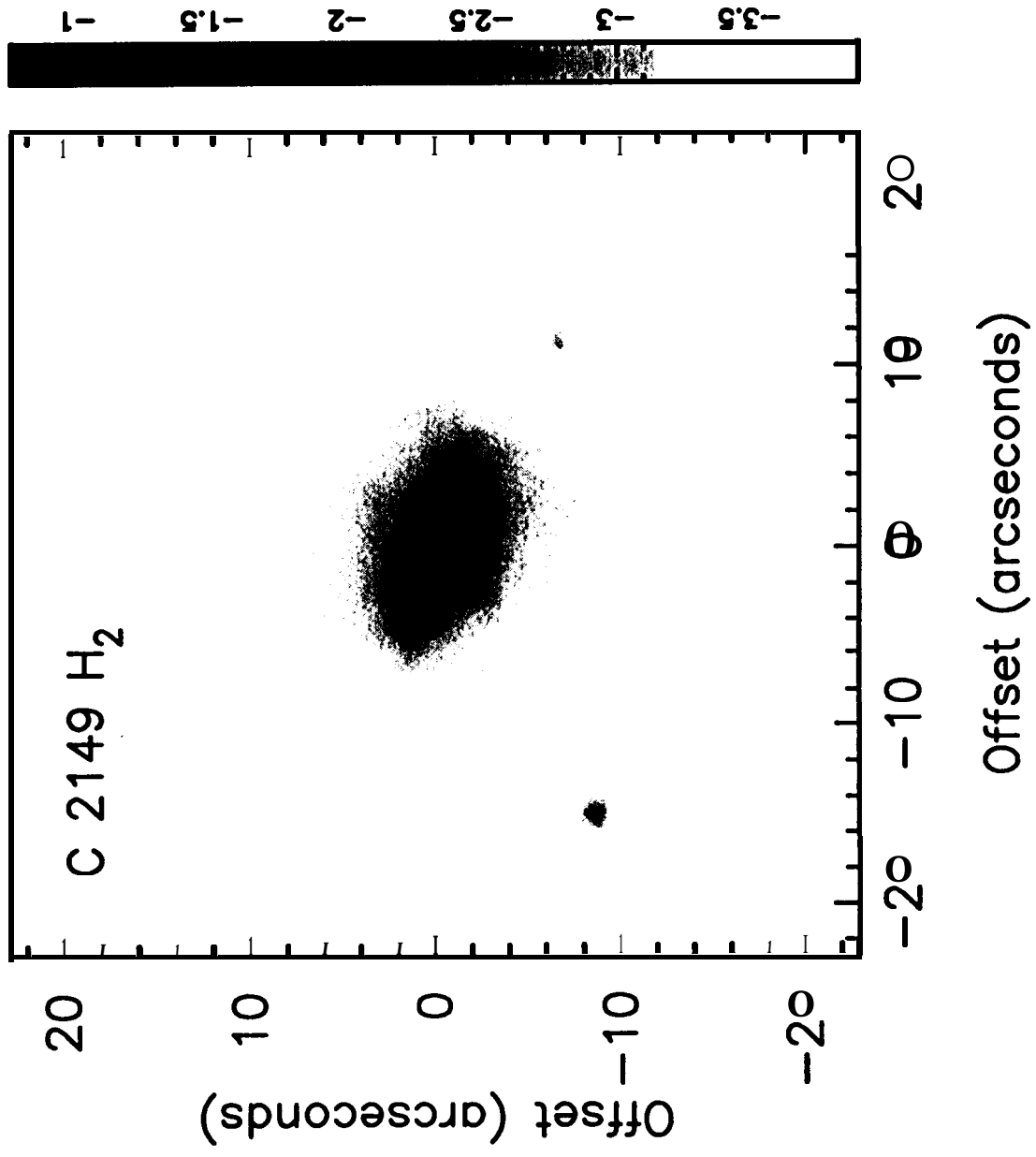
Offset (arcseconds)

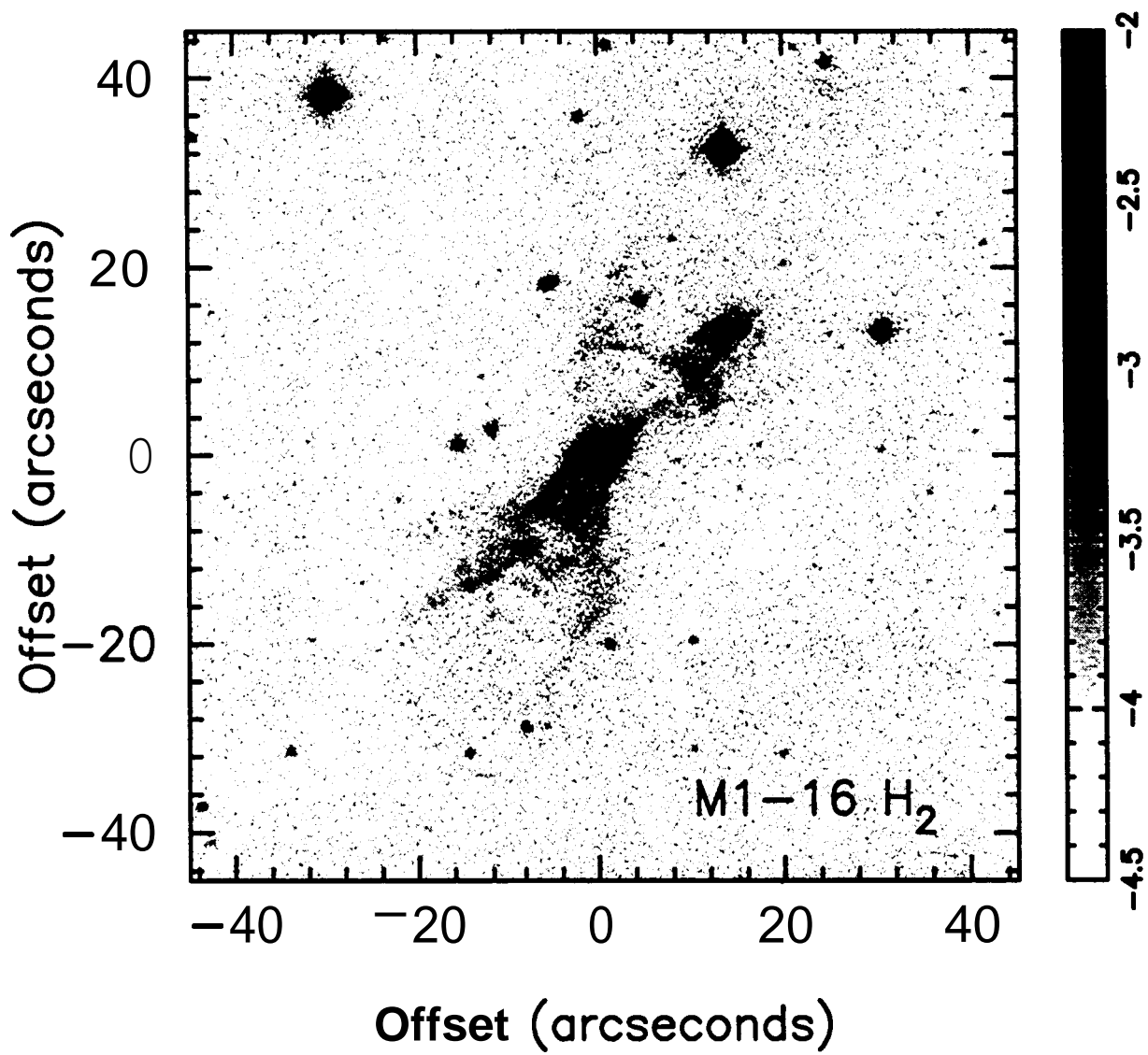


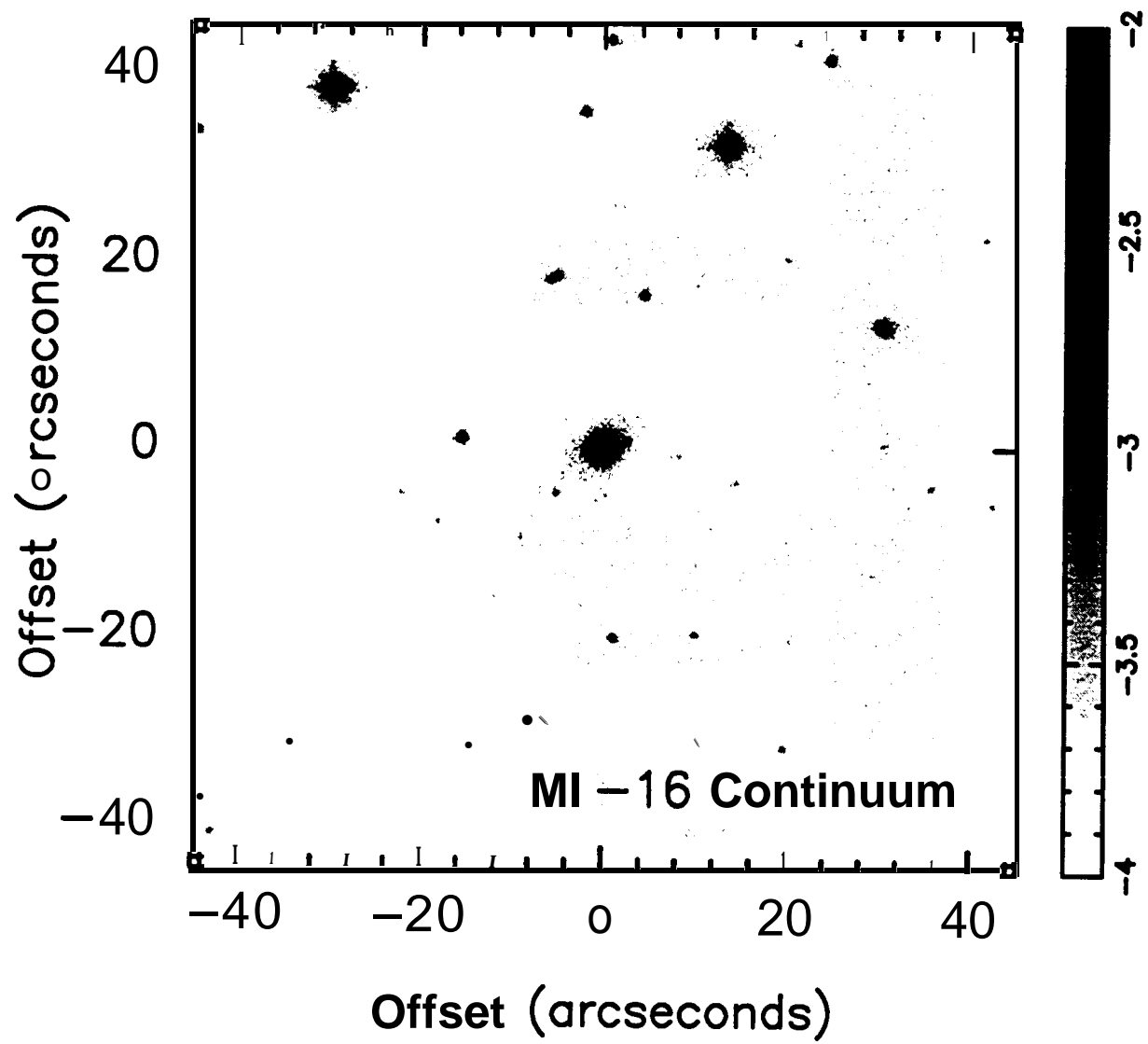
Offset (arcseconds)

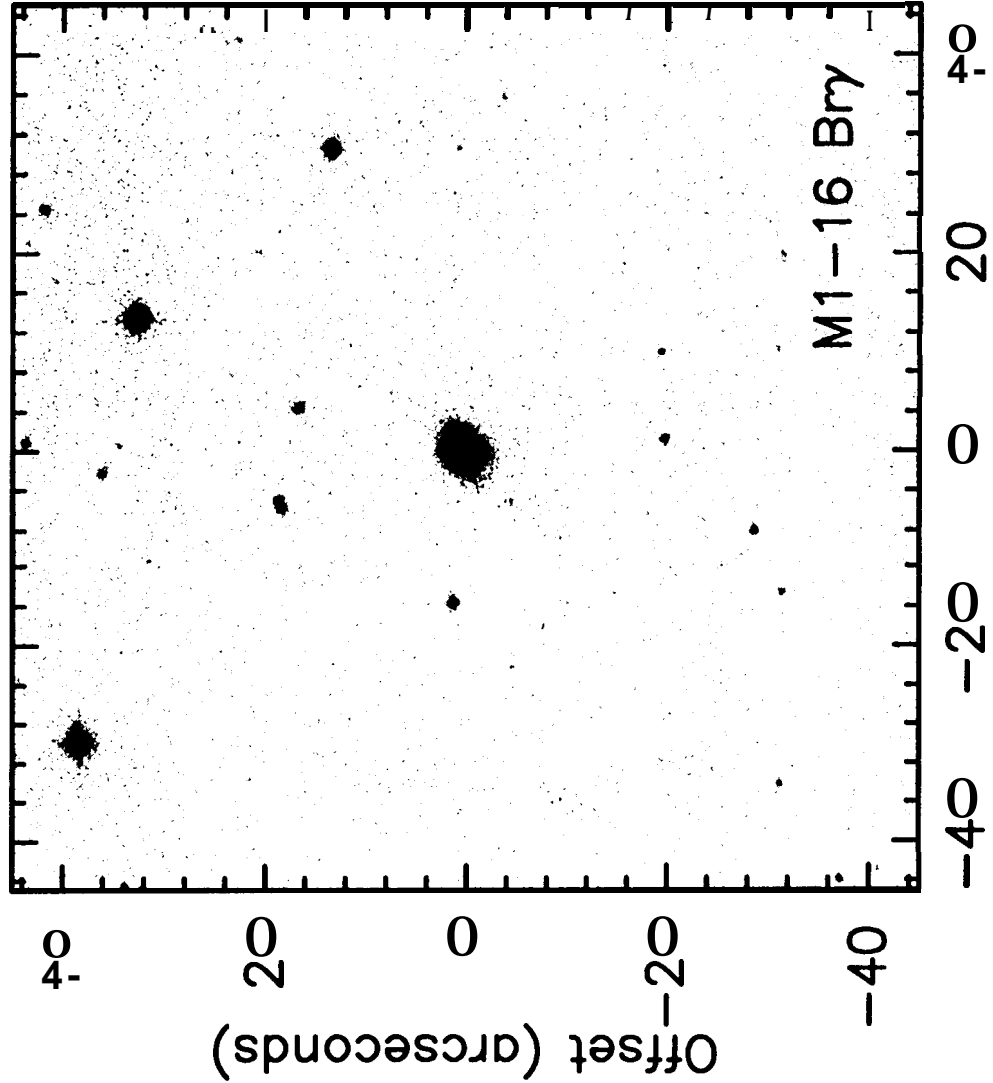












Offset (arcseconds)

